# ENVISAT — TAKING THE MEASURE OF NORTH ATLANTIC STORMS

**Graham D. Quartly[1] , Caroline A. Poulsen[2] & Trevor H. Guymer[1]**

[1] *National Oceanography Centre, Southampton, Empress Dock, Southampton,*
*Hants, SO14 3ZH, UK.  email: gdq / thg @noc.soton.ac.uk*
[2] *Rutherford Appleton Laboratory, Chilton, Didcot, Oxon, OX11 0QX, UK. email: c.a.poulsen@rl.ac.uk*

## ABSTRACT

*Envisat* carries a number of sensors able to provide quantitative information on raining clouds: AATSR delivers information on cloud microphysics (particle size, temperature etc.), MWR-2 gives columnar totals for liquid and vapour forms of water, and RA-2 yields rain rate and wind speed.  This paper examines the complementarity of these sensors, with a focussed study on significant rain events in the N. Atlantic, covering both coherent large storms and fronts with smaller scale structure.  The difference in liquid water estimates from the infra-red and passive systems appears to be related to the temperature and sizes of drops being detected.

## 1. INTRODUCTION

Rain, whether as frontal activity or in large storm systems, is an important factor in ocean-atmosphere interaction, with strong latent heat release affecting atmospheric dynamics, and freshwater input adjusting the surface salinity of the ocean, with potential impacts on subsequent circulation.  Also, nearly all of the tropical storms and hurricanes to reach the east coast of N. America have originated over the tropical Atlantic, so study of the structure and evolution of storms in the Atlantic are key to better understanding and prediction of their eventual intensity and tracks.  In an earlier paper [1], we considered six disturbances in the Gulf of Guinea, the genesis region for many hurricanes; more recently we identified 10 major events in a 30-day period over the western N. Atlantic (see Fig. 1).  One of these events, Hurricane Juan, has been analysed in detail [2]; here we consider two other case studies.

## 2. DATA

As rain systems evolve rapidly, combining information from different satellites can be problematic.  Here we make use of the simultaneous observations by three *Envisat* sensors to provide a more complete look at raining clouds than could be achieved with a single sensor.

The dual-frequency altimeter, RA-2, gives estimates of wave height and backscatter strength ($\sigma^0$)

at $K_u$-band and S-band.  $K_u$-band processing has the longer heritage, so standard algorithms for wind speed use $\sigma^0_{Ku}$; however when rain is present $\sigma^0_S$ is more robust, and the difference in behaviour at the two frequencies provides an estimate of the attenuation and hence rain rate.

The passive microwave radiometer, MWR-2, records brightness temperatures (BT) at two frequencies (23.8 and 36.5 GHz), with a record of sea surface roughness provided by $\sigma^0_{Ku}$ being used in the inversion [3] to give columnar totals of water vapour (WV) and liquid water content (LWC).  Again, because of the sensitivity of $\sigma^0_{Ku}$ to rain, improved performance in such conditions can be achieved by using $\sigma^0_S$ [2].

The infra-red radiometer, AATSR, provides high-resolution (1 km) sampling across a 512 km swath, using 7 channels; of these the five longest wavelengths (0.87, 1.6, 3.7, 11 & 12 μm) are combined through a radiative transfer model [4] to give optical depth (OD), cloud top height (CTH), cloud top temperature (CTT), mean particle size ($r_0$) and liquid water path (LWP).  Details on the required processing are given in our earlier works [1,2]; in this short paper we concentrate on the analysis of our selected case studies.
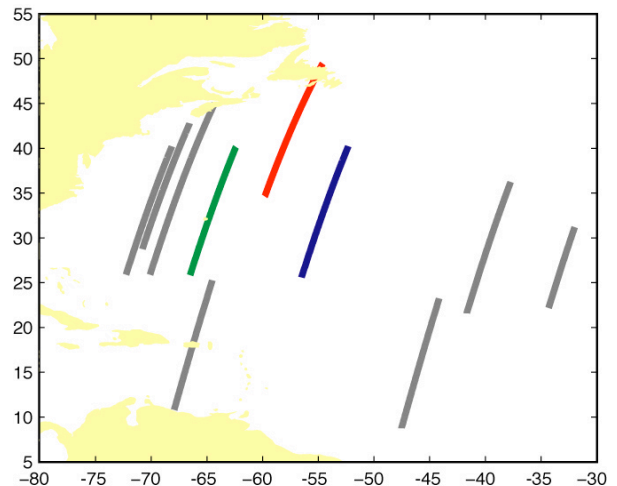


*Figure 1: Locations of the 10 western N. Atlantic events identified during the 30-day study period (Sept./Oct. 2003).   The track in green covers Hurricane Juan [2]; the blue line is across the large storm of section 3.1 of this paper and the red line covers the frontal activity of section 3.2.*

## 3. INDIVIDUAL CASE STUDIES

The three sections emphasised in Fig. 1 have been examined in detail. The one highlighted in green is through Hurricane Juan, a category-2 hurricane, which *Envisat* overflew whilst the storm was near Bermuda, 2 days before it made landfall at Halifax, Nova Scotia. The event marked by a blue line is another large organised storm (see Fig. 2); whilst the red line in Fig. 1 shows a transect across a smaller scale frontal disturbance (see Fig. 3).
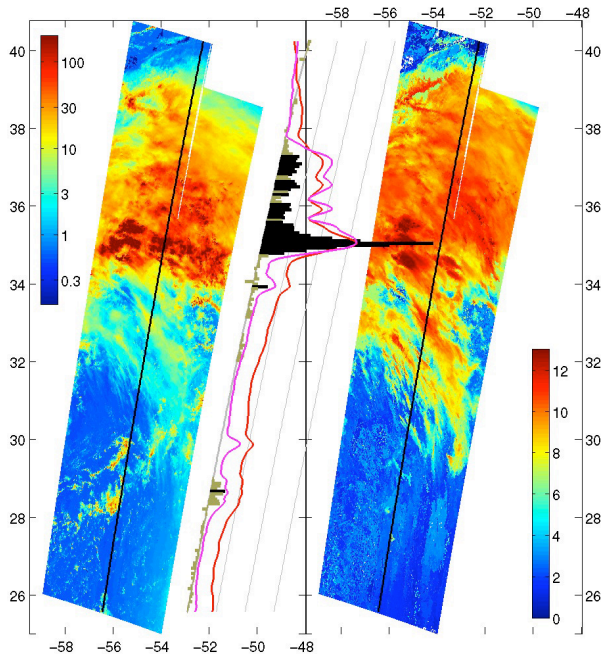


*Figure 2: Illustration of multi-sensor data across a storm event. Left-hand panel shows optical depth and right-hand one cloud top height, both from the AATSR. The horizontal lines in the middle show attenuation observed by the RA-2 (in black when statistically significant), and the pink and red lines are the 24 & 36 GHz brightness temperatures from the MWR-2 (relative to a base line of 170 K).*

### 3.1 Event 1 : A storm event

The display of cloud top height (right-hand panel of Fig. 2) shows a large storm system spanning 34° to 39°N, with a cloud top height at ~11 km. However the optical depth, a measure of the thickness of the cloud shows the system to be much more dense at its southern limit, with a reduction by a factor of three by 39°N. To the south of the storm are streaks of high level cirrus, which are remnants of previous activity (as shown by MODIS imagery).

The attenuation signal in the middle panel corresponds to heavy rain at 35°N, with light rain for the 250 km further north, characteristic of an active frontal system. The coarser resolution BT values from the passive microwave sensor confirm this latitudinal profile. At 28.5°N there are several cells of activity; although CTH is only 4 km, the cloud is the densest south of 34°N and is marked by significant rain.

The left-hand panels of Fig. 4 show the profiles of geophysical retrievals from all 3 sensors along the satellite track. The AATSR products have been averaged over the appropriate altimeter footprints (~8 km diameter disks every 6.7 km along track). The significant wave height (SWH) at $K_u$-band shows a fairly uniform value of 2 m (close to the mean global value); this suggests that there have not been strong winds blowing for a long time. The sharp peak in SWH is a spurious feature due to variable attenuation by rain affecting the altimeter waveforms [5]. The S-band values do show spatial variation, coinciding with the peak in wind speed, although S-band wave heights are generally thought less reliable.

### 3.2 Event 2 : Frontal activity

Figure 3 portrays an *Envisat* pass running obliquely across a system within which there is smaller scale organization, in the form of small core cells (see left-hand panel). The rain (as evidenced by the RA-2 attenuation) occurs in small localised patches too.
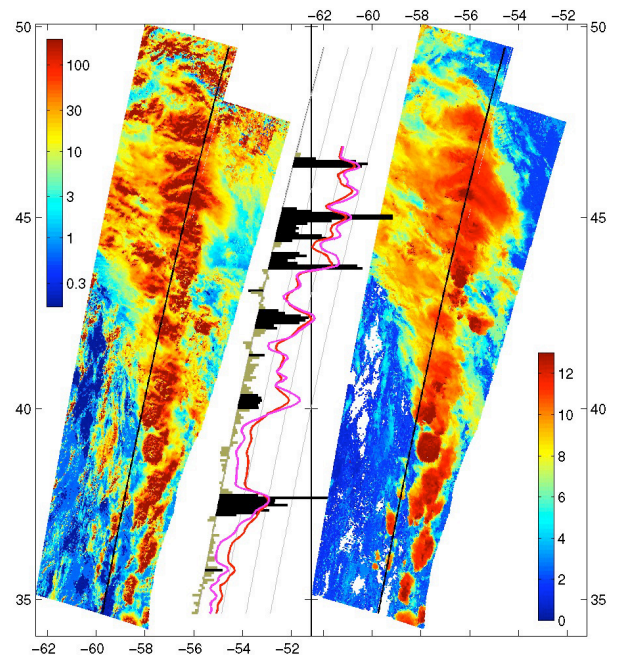


*Figure 3: Same as Fig. 2 but for a frontal event. (Note there are no RA-2 or MWR-2 data north of 47°N, because that is over Nova Scotia.)*
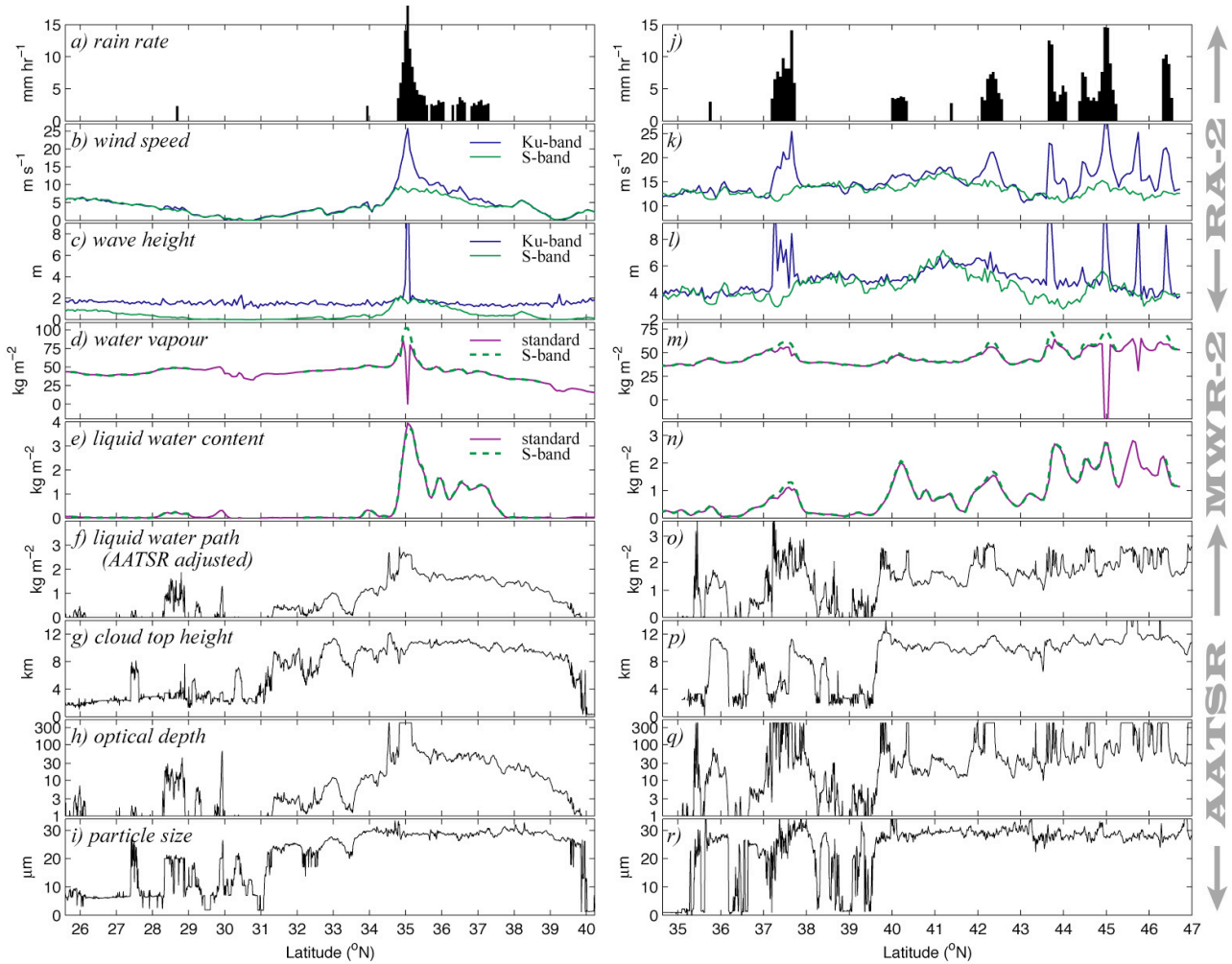
*Figure 4: Profiles of geophysical parameters along the nadir track for storm event (left hand-panels) and frontal event (right-hand). The two lines in each of b), d) and e) [and also k), m) and n)] show the effect of using $\sigma^0_S$ in place of $\sigma^0_{Ku}$ in the standard inversion code. (Wave height using S-band data is a standard product, although the values are usually too noisy to use.)*

Interestingly the SWH profile (Fig. 4l) shows values of 4-6 m, peaking at 41°N, at the centre of the section shown. S-band estimates agree much better than in the previous case (Fig. 4c). The wind speeds are also greater across this event, with the $K_u$-band values again being biased high when rain is present. Only two of the rain features lead to wildly erroneous WV estimates (45.0° & 45.8°N), but in several other cases the derived WV loading is less than that inferred using $\sigma^0_S$ (e.g. 43.8° & 46.5°N).

The AATSR-derived parameters show fairly uniform values north of 39.5°N, with the variations further south being due to sampling of discrete cells. Note the feature at 35.8°N, which is relatively narrow in both directions (see Fig. 3), but is intense enough to have an active rain field associated with it (Fig. 4j).

Quartly & Guymer [2] had identified that rain-affected estimates of $\sigma^0_{Ku}$ led to spurious WV & LWC values at the centre of Hurricane Juan; these additional two case studies confirm those findings. They had also drawn attention to the significant differences between the profiles of LWC and LWP, essentially the same quantity estimated from MWR-2 and AATSR respectively; these differences are explored further in the next section.

## 4. LWC AND LWP

The AATSR estimates of LWP have had to be adjusted by a factor of ten for consistency; after that there is broad general agreement in the values of LWC and LWP with the positioning of many features being in common. However, in Figs. 4e & 4f for instance, the shapes of the profiles between 36° and 40°N are very different, and the feature around 28.7°N has a very weak LWC signature, due, at least in part to the MWR's much broader footprint.

These differences in the quantitative records are conjectured to be caused by the relative sensitivities of these different wavebands (infra-red versus microwave) to drop sizes and temperatures. To clarify this, various cluster plots were constructed (Fig. 5), with the LWP values averaged over a footprint size equivalent to that of MWR-2. Note both algorithms occasionally produce negative output, which is not physically meaningful; these are left on the plots to indicate the circumstances in which they occur.

The top plot shows the overall envelope of match-ups in grey, with the two case studies distinguished by colour. The whole cluster is crescent-shaped, with the infra-red measure (LWP) responding more rapidly at low values to the presence of atmospheric liquid water, and then as that indicator saturates the microwave one (LWC) continues to show a response. This crescent nature was even more pronounced with the unsmoothed LWP data (not shown), as small cells could strongly affect LWP without making much effect on the LWC record. Although the first case seems to show a progression through LWP-LWC space, with LWP values being relatively low (less than 2.0) on the south side of the storm, and then relatively high (>2.3) on the north side, there is no clear pattern for the second case (which has multiple rain patches), with the LWP value changing markedly between successive points.

The other three cluster plots show how various other parameters — mean particle size, CTT and rain rate — affect the population of LWC-LWP space. Not surprisingly each analysis shows some separation along the broad crescent: increased atmospheric liquid water (as recorded by both LWC and LWP) is associated with more active rain-bearing systems, typically having larger particles (Fig. 5b), higher and colder cloud tops (Fig. 5c) and increased rain rate (Fig. 5d). However within each grouping there is still much scatter. Within the observations eliciting minimal microwave response (LWC<0.5 kg m$^{-2}$), it appears that the infra-red-derived measure, LWP, increases most when particle size is large ($r_0$>25 μm) and there are high clouds (CTT<265 K). However, as these values also come from the AATSR rather than an independent source, there may be correlated errors in their estimates. An initial look suggests that of these three measures CTT may best explain the observed differences between LWP and LWC, but firm conclusions await further analysis, probably with a larger number of events.

## 5. SUMMARY

Many sensors show a response to raining clouds, and can be used to give quantitative values across them; *Envisat* brings together three very different instruments (infra-red radiometer, microwave radiometer and an active microwave sensor) to record complementary characteristics of these rain systems. Here we have built on previous work [1,2] to include two detailed case studies — one across a large organised system and the other dominated by much more small-scale structure. However, many of the findings were the same. Rain's effect on $\sigma^0_{Ku}$ not only leads to unreasonable large wind speed estimates, but can cause the neural net governing WV retrievals to give low or even negative values. The effect on LWC is negligible.
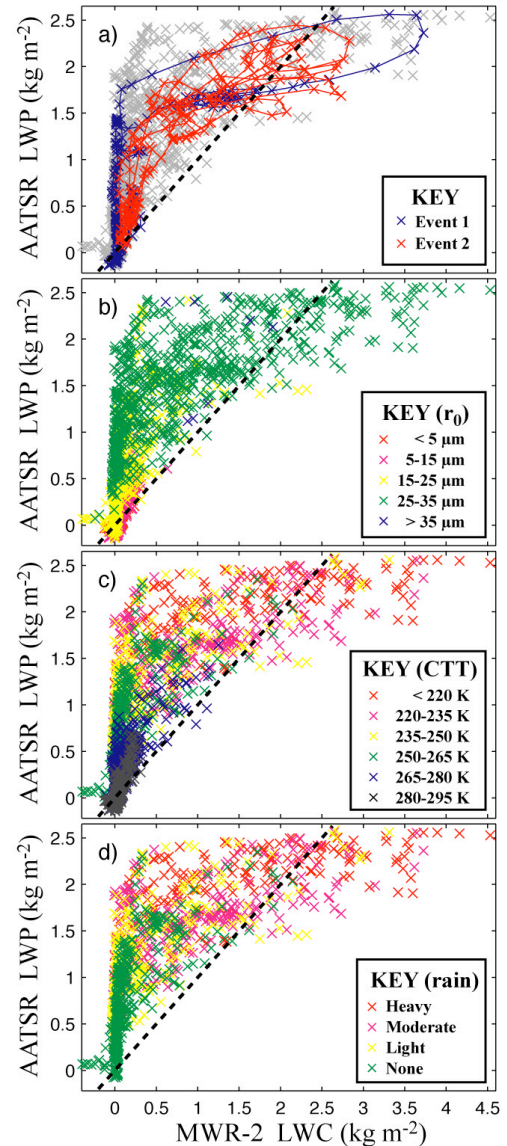


*Figure 5: Cluster plots showing factors affecting the differences in columnar liquid water estimates from microwave and infra-red sensors, with both values calculated over similar footprints. Coloured by a) case study, b) particle size, c) cloud top temperature, and d) rain rate.*

For both events, some AATSR-derived parameters such as CTH and $r_0$ remained reasonably constant at high levels on the northern part of the section, but showed much more spatial variation in the southern stretches. Not all the nadir-track features present in the AATSR product had an appreciable signature in the microwave records.

In particular, although showing some similarities, there were marked differences between the microwave and infra-red estimates of atmospheric liquid water. These were investigated through cluster plots, which showed LWP to respond initially more rapidly than LWC, but then suffer from saturation, allowing LWC to give the highest values. The resulting crescent distribution implies that at least one of the instruments is not accurately recording the conditions; on the other hand, Fig. 5 suggests a complementary nature for liquid water retrievals from these two sensors, with the MWR providing gradations in data when the AATSR measure is saturated. Further work is required to understand fully these differences between LWC and LWP.

LWP values exceeding $1 \, \mathrm{kg \, m^{-2}}$ are frequently found with little or no rain present, whereas LWC values over this threshold are usually associated with rain. Quartly & Guymer [2] concluded that the necessary conditions for rain were OD>6 *and* LWC>1 (i.e. that the microwave-based measure provided the more useful discriminator in that context).

## 7. REFERENCES

1. Quartly, G.D & Poulsen, C.A. (2005). Coincident cloud observations by altimetry and radiometry, *Proc. of Envisat & ERS Symposium, Salzburg, 6-10th Oct. 2004*, ESA SP-572 (5pp).
2. Quartly, G.D. & Guymer, T.H. (2007). Realizing Envisat's potential for rain cloud studies, *Geophys. Res. Lett.*, 34, art. no. L09807 doi: 10.1029/2006GL028996.
3. Obligis, E., Eymard, L., Tran, N., Labroue, S. & Femenias, P. (2006). First three years of the Microwave Radiometer aboard Envisat: In-flight calibration, processing and validation of the geophysical products, *J. Atmos. Oceanic Tech.*, 23, 802-814, 2006.
4. Watts, P.D. et al. (1998). Study on cloud properties derived from Meteosat Second Generation observations, EUMETSAT ITT no. 97/181.
5. Quartly, G.D. (1997). Achieving accurate altimetry across storms: Improved wind and wave estimates from C-band, *J. Atmos. Oceanic Tech.* 14, 705-715.